SUPPORTING INFORMATION

Stabilization of nanoparticles produced by hydrogenation of Palladium-NHC complexes on the surface of graphene and implications in catalysis

Andrés Mollar-Cuní,[a] David Ventura-Espinosa,[a] Santiago Martín,[b,c] Álvaro Mayoral,[d,¶] Pilar Borja[*a] and Jose A. Mata[*a]

[a]Institute of Advanced Materials (INAM), Universitat Jaume I, Avda. Sos Baynat s/n, 12006, Castellón (Spain). Fax: (+34) 964387522; Tel: (+34) 964387516; e-mail: jmata@uji.es

[b]Departamento de Química Física, Facultad de Ciencias, Universidad de Zaragoza, C/Pedro Cerbuna 12 50009 Zaragoza (Spain).

[c]Instituto de Ciencias de Materiales de Aragón (ICMA), Universidad de Zaragoza-CSIC, 50009 Zaragoza (Spain).

[d]Instituto de Nanociencia de Aragón (INA) and Laboratorio de Microscopias Avanzadas (LMA), edificio i+d Campus Río Ebro, Universidad de Zaragoza, C/Mariano Esquillor, s/n, 50018 Zaragoza (Spain).

Contents

S1. Experimental

General procedures. Solvents were dried using a solvent purification system. Nuclear magnetic resonance (NMR) spectra were recorded on Bruker spectrometers operating at 300 or 400 MHz (^{1}H NMR) and 75 or 100 MHz (^{13}C{^{1}H} NMR), respectively, and referenced to $SiMe_4$ (δ in ppm and J in Hertz). NMR spectra were recorded at room temperature with the appropriate deuterated solvent. High-resolution images of transmission electron microscopy HRTEM and high-angle annular dark-field HAADF-STEM images of the samples were obtained using a Jem-2100 LaB6 (JEOL) transmission electron microscope coupled with an INCA Energy TEM 200 (Oxford) energy dispersive X-Ray spectrometer (EDX) operating at 200 kV. Samples were prepared by drying a droplet of a MeOH dispersion on a carbon-coated copper grid. X-ray photoelectron spectra (XPS) were acquired on a Kratos AXIS ultra DLD spectrometer with a monochromatic Al Kα X-ray source (1486.6 eV) using a pass energy of 20 eV. To provide a precise energy calibration, the XPS binding energies were referenced to the C1s peak at 284.6 eV. TGA analysis were performed using a TG-STDA Mettler Toledo model TGA/SDTA851e/LF/1600 coupled to a mass spectrometer quadrupol PFEIFFER VACUUM model OmniStar GSD 320 O3, 1-300 uma. bearing tungsten filament.

General procedure for the catalytic hydrogenation of alkynes:
In a general catalytic experiment, a 10 mL schlenk equipped with a stirring bar is charged with 0.3 mmol of alkyne, base (Cs_2CO_3, 10 mol %), catalyst (1 mol % for **2** and 0.5 mol % for **2-rGO**) and 2 mL of dry toluene as solvent. A balloon full of H_2 is conected to the schlenk. The schlenk is then introduced in a preheated 65 ^{o}C oil bath. Yields and conversions were determined by GC or ^{1}H NMR analysis using anisole or 1,3,5-trimethoxybenzene as internal standard.

S2. Nuclear Magnetic Resonance (NMR) Analysis

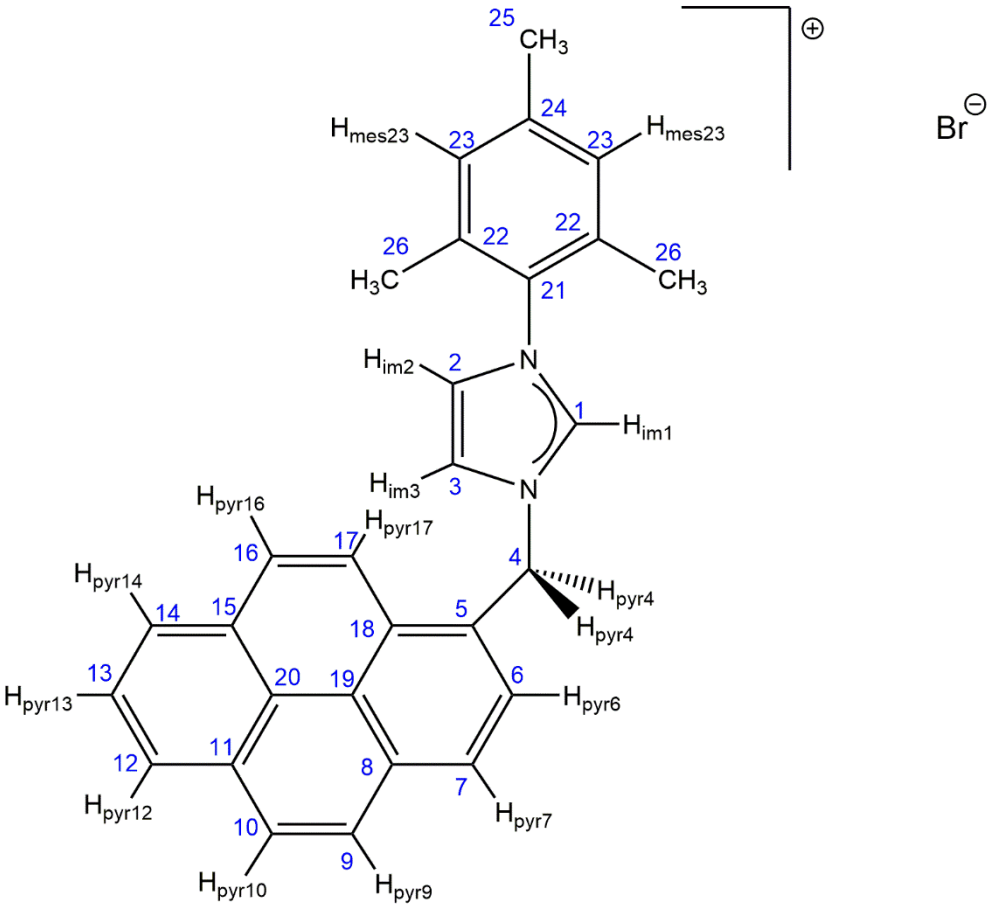

Figure S1 Numbering scheme for imidazolium salt **1**.

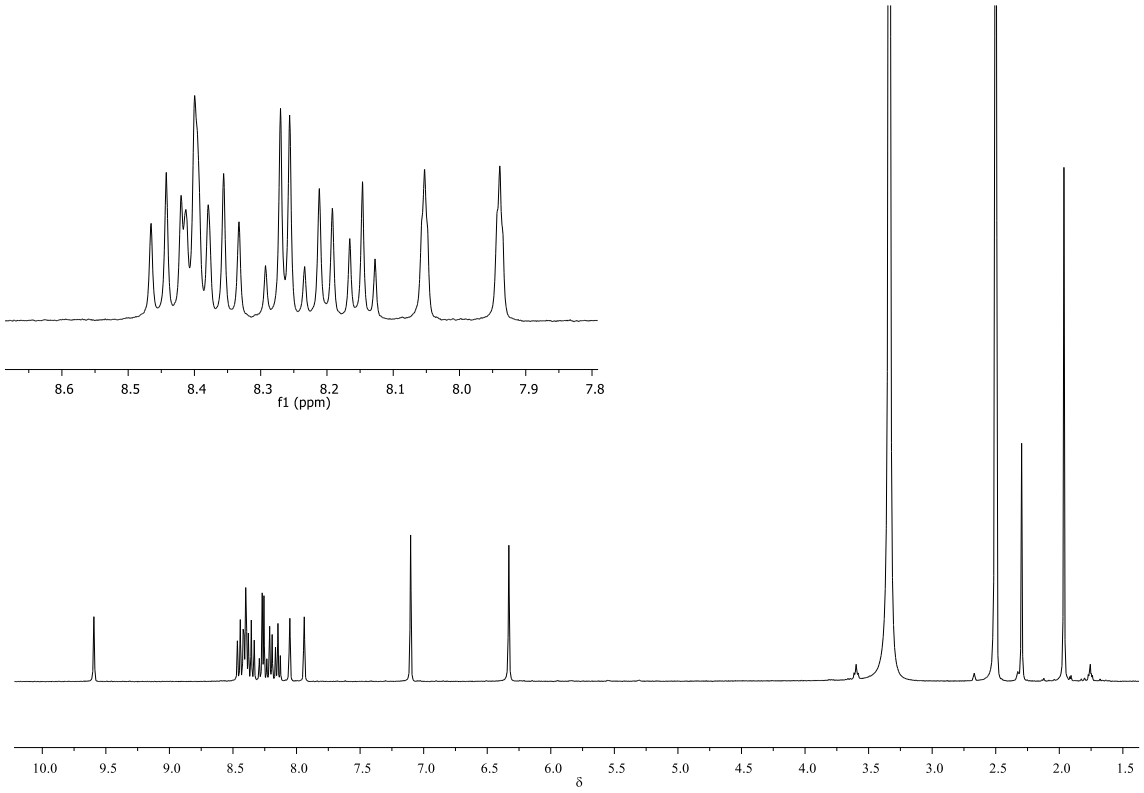

Figure S2 ^{1}H NMR spectrum of imidazolium salt **1** in DMSO-d6.

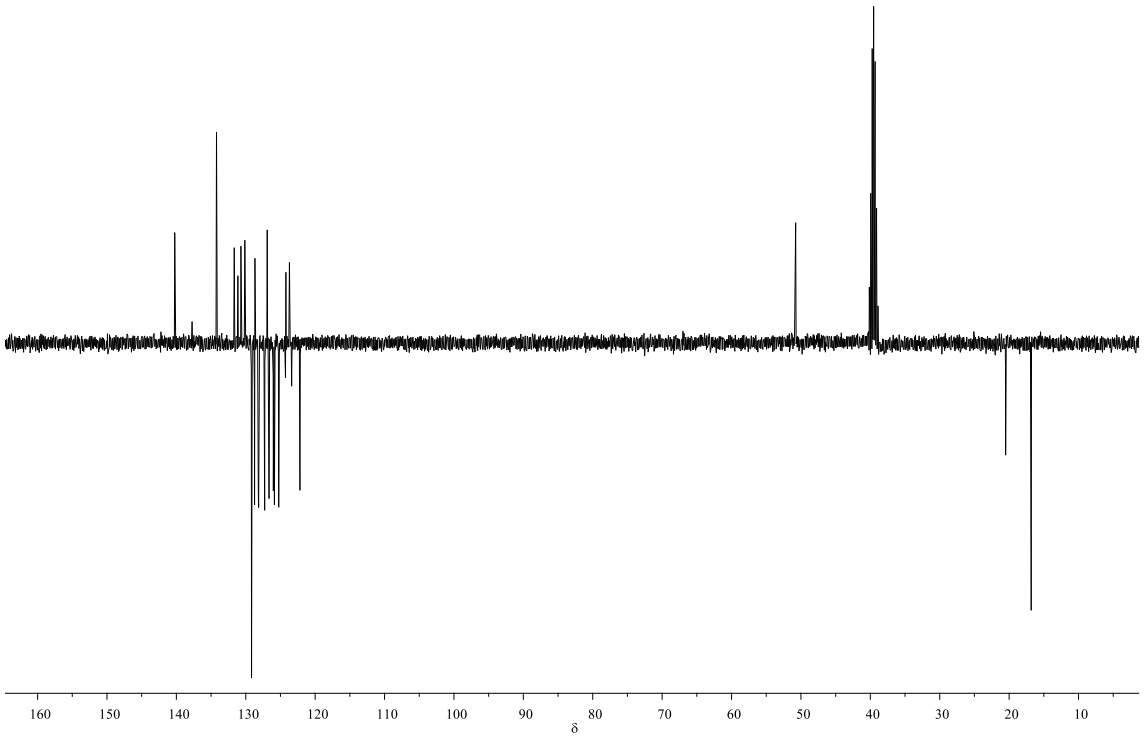

Figure S3 APT spectrum of imidazolium salt **1** in DMSO-d6.

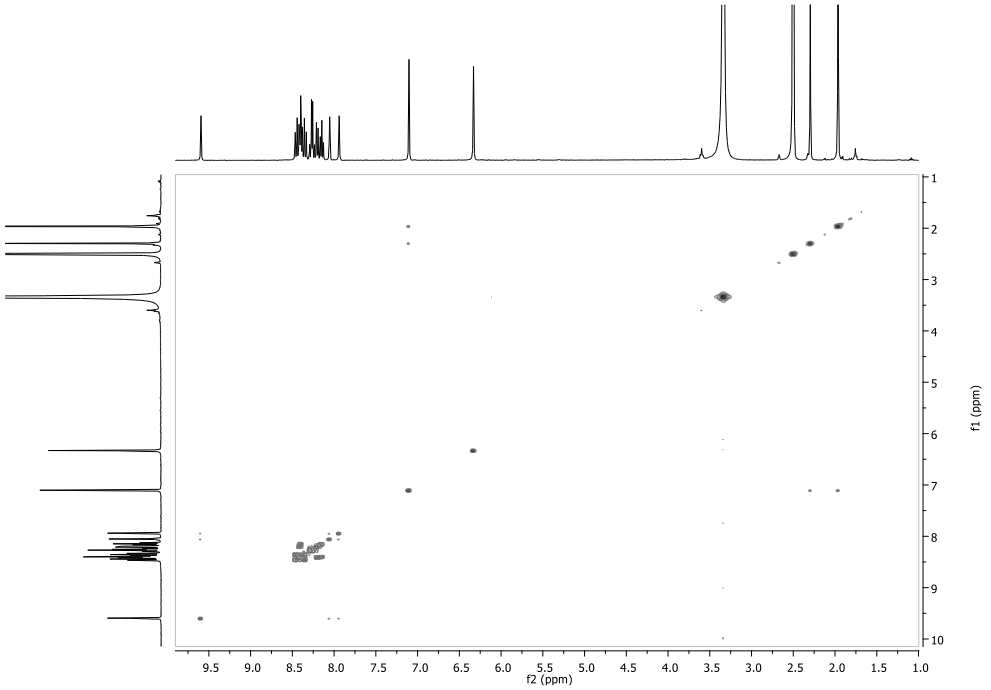

Figure S4 (^{1}H-^{1}H)-COSY spectrum of imidazolium salt **1** in DMSO-d6.

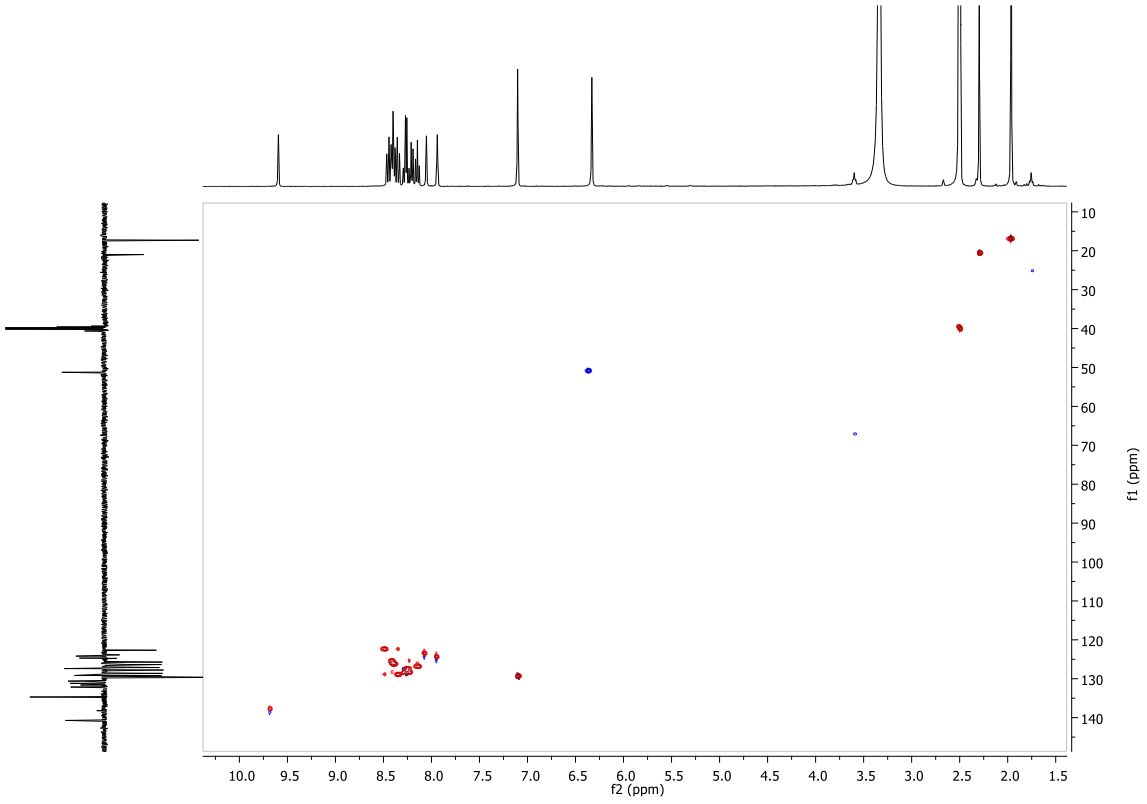

Figure S5 (^{1}H-^{13}C)-HSQC edited of imidazolium salt **1** in DMSO-d6 (CH, CH_3 in red, CH_2 in blue).

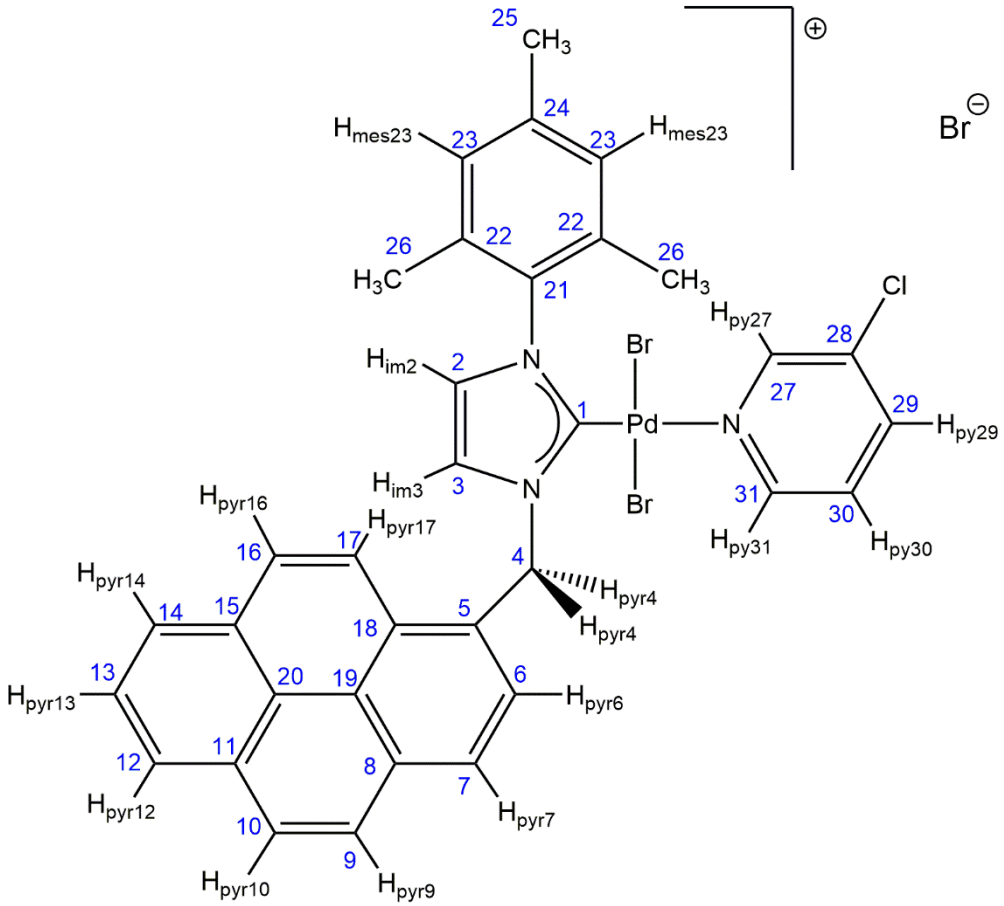

Figure S6 Numbering scheme of molecular complex **2**.

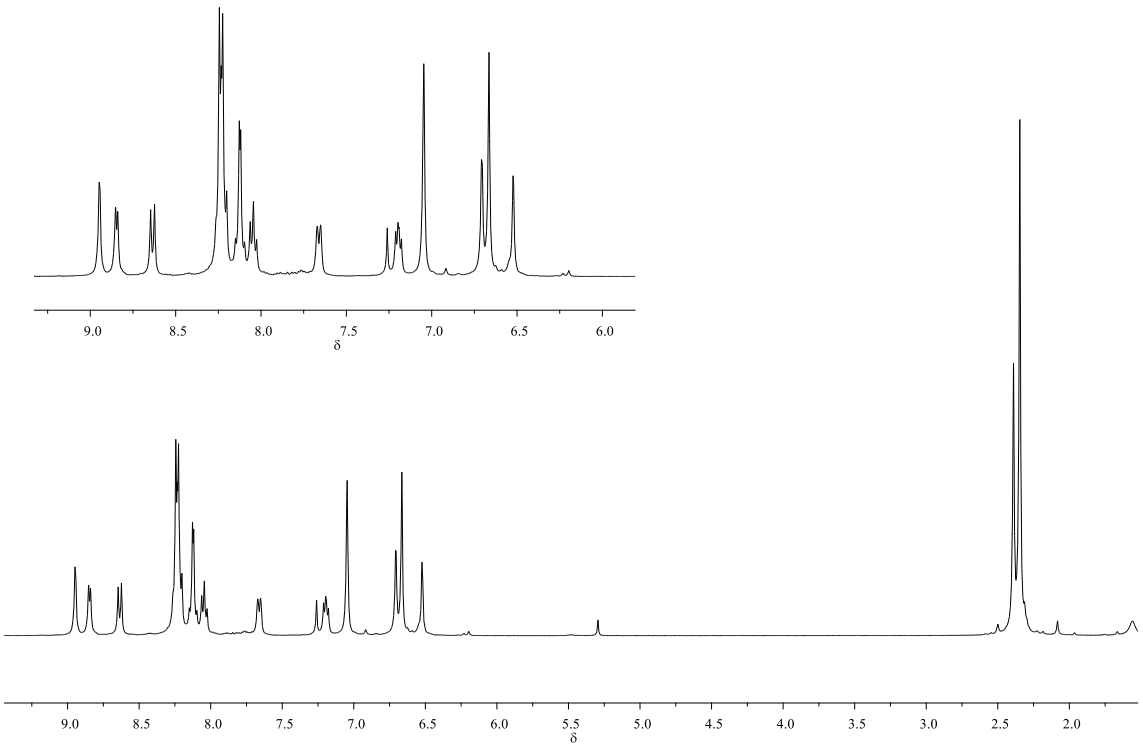

Figure S7 ^{1}H-NMR spectrum of complex **2** in $CDCl_3$.

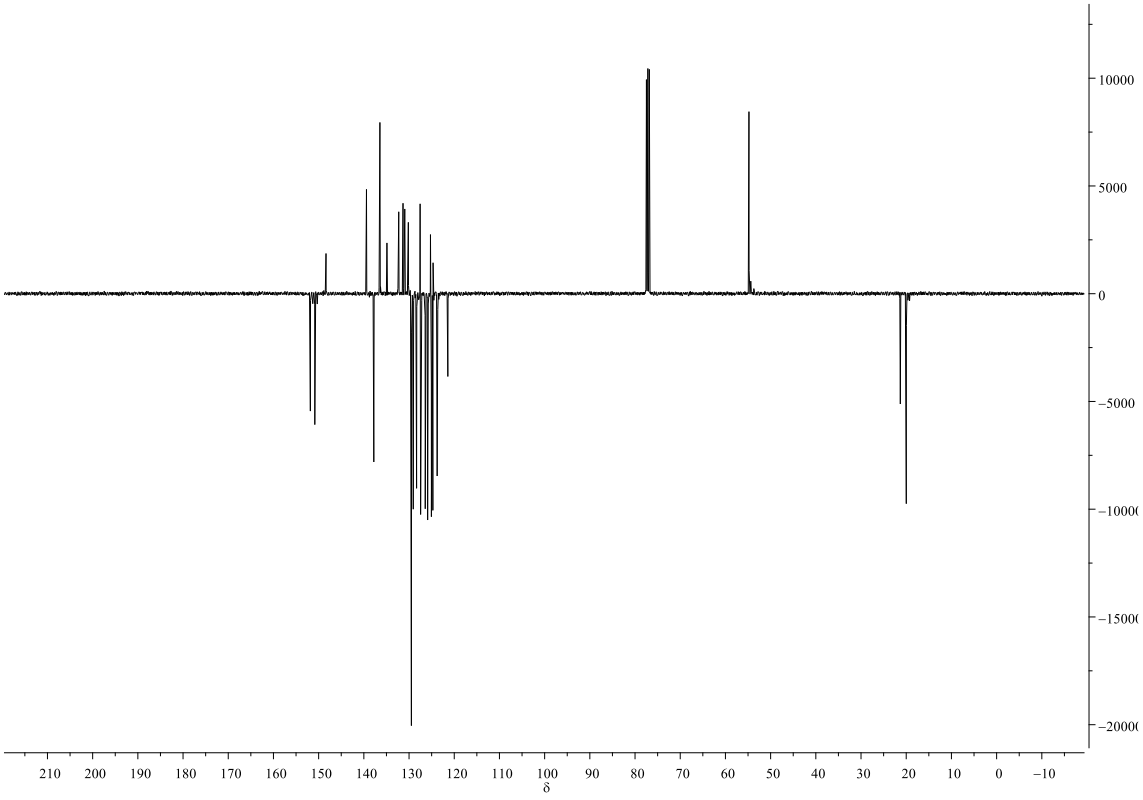

Figure S8 APT spectrum of complex **2** in $CDCl_3$.

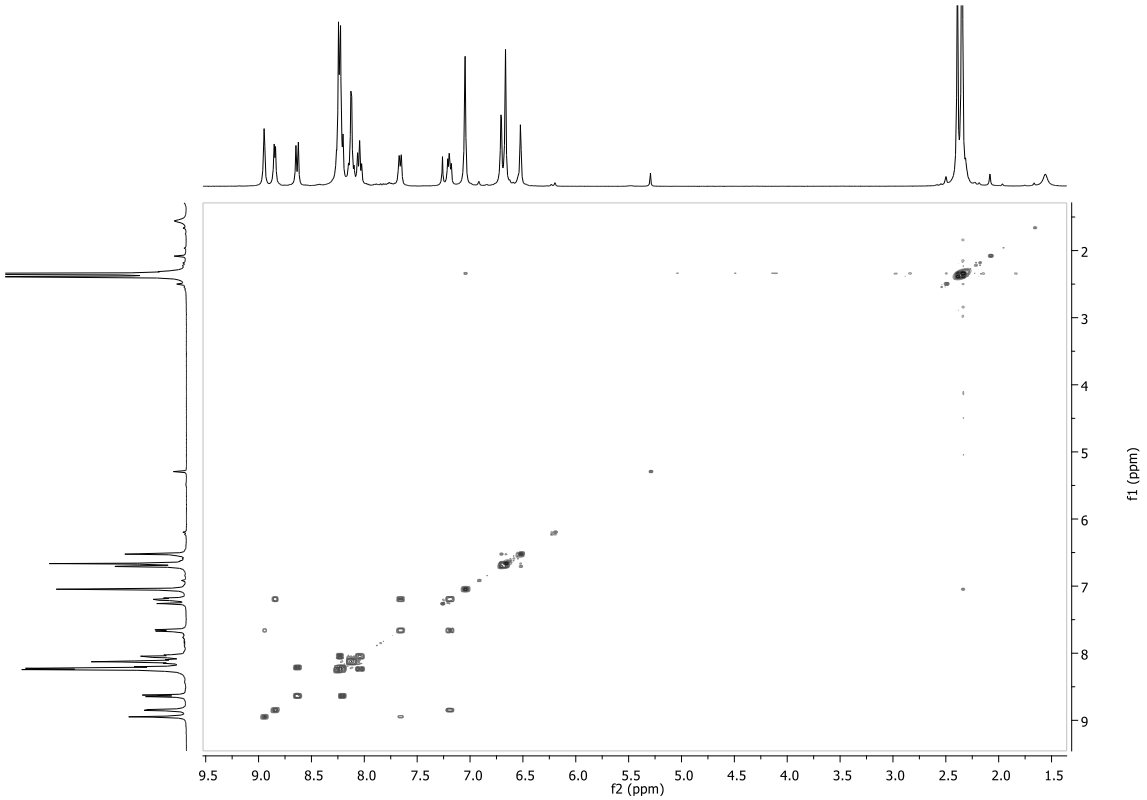

Figure S9 (^{1}H-^{1}H)-COSY spectrum of complex **2** in $CDCl_3$ (CH, CH_3 in red, CH_2 in blue).

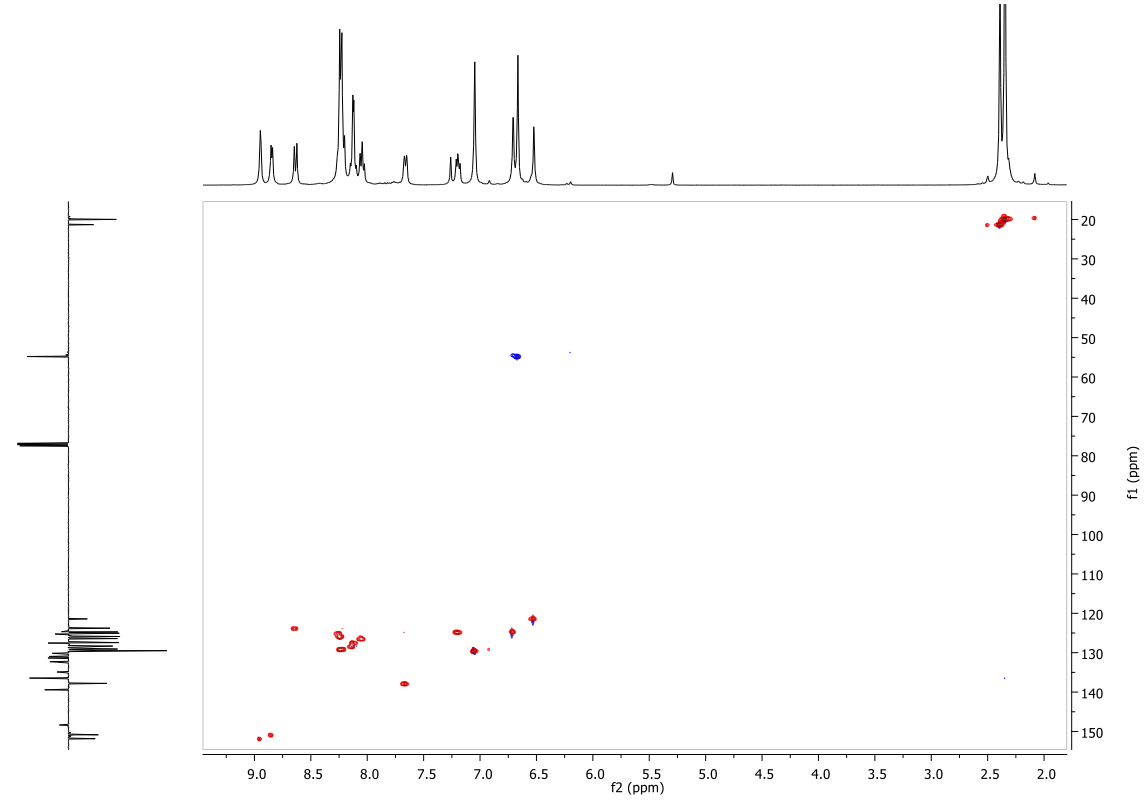

Figure S10 (^{1}H-^{13}C)-HSQC edited of complex **2** in $CDCl_3$.

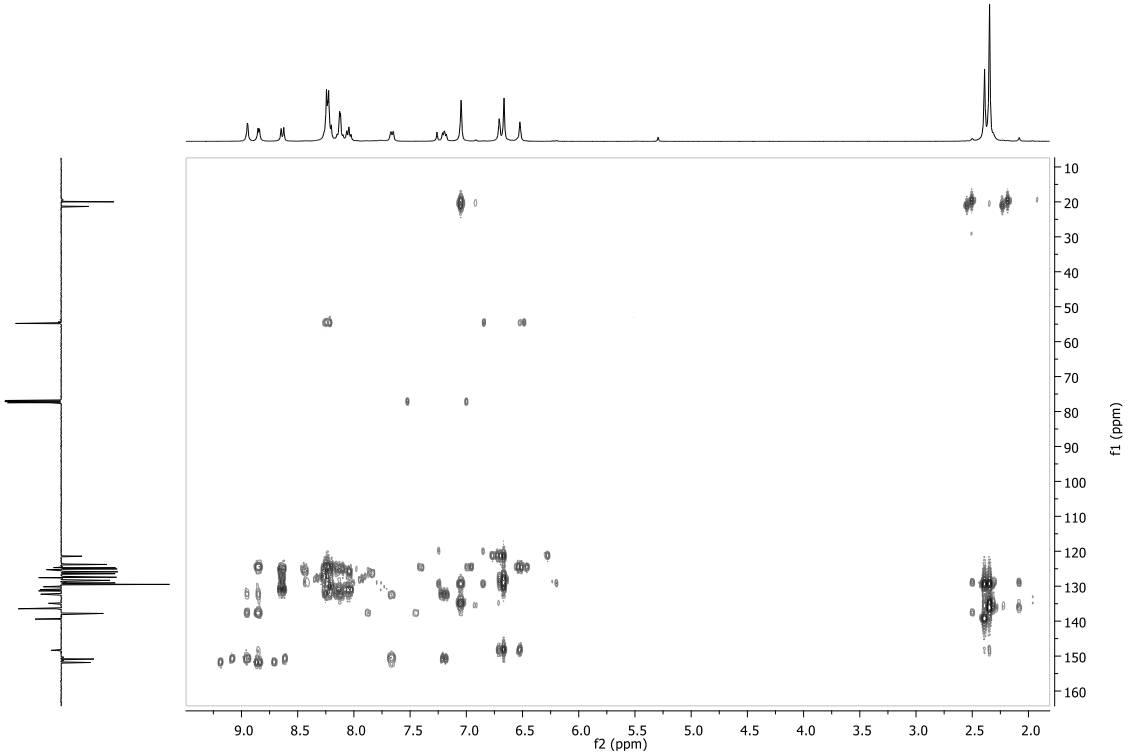

Figure S11 (^{1}H-^{13}C)-HMBC spectrum of complex **2** in $CDCl_3$.

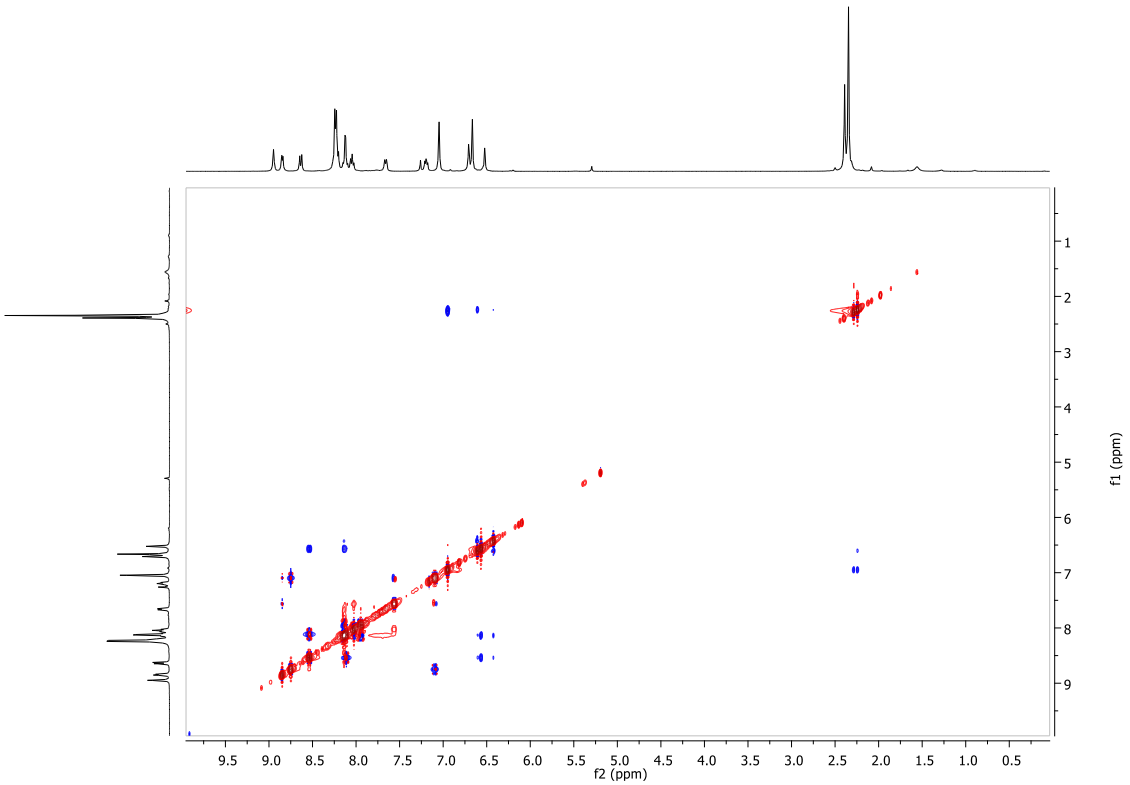

Figure S12 (^{1}H-^{1}H)-NOESY spectrum of complex **2** in $CDCl_3$.

Complete hydrogenation of diphenylacetylene with **2** (t = 3h):

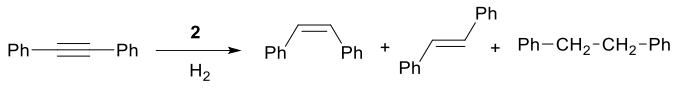

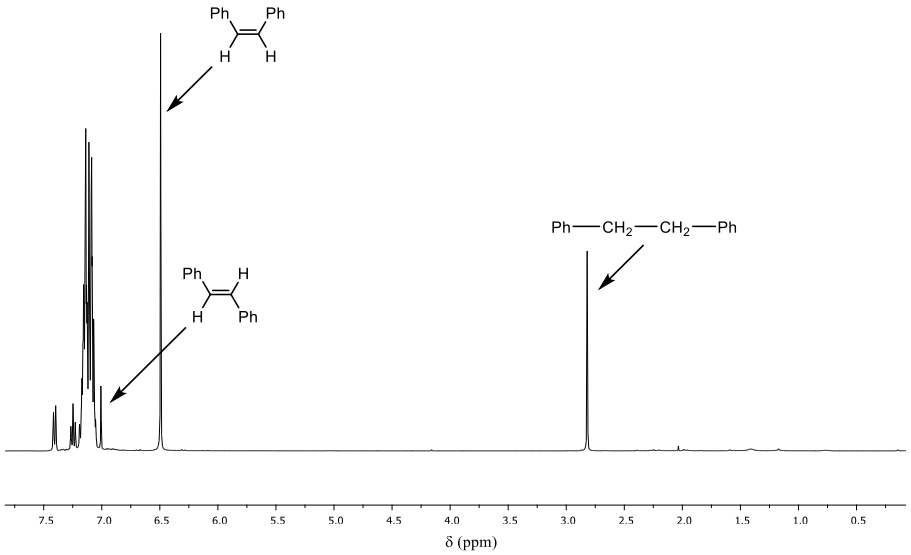

Complete hydrogenation of diphenylacetylene with **2-rGO** (t= 3.5h):

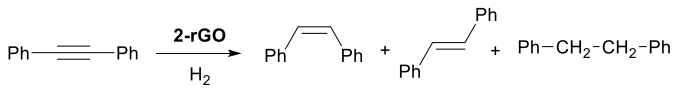

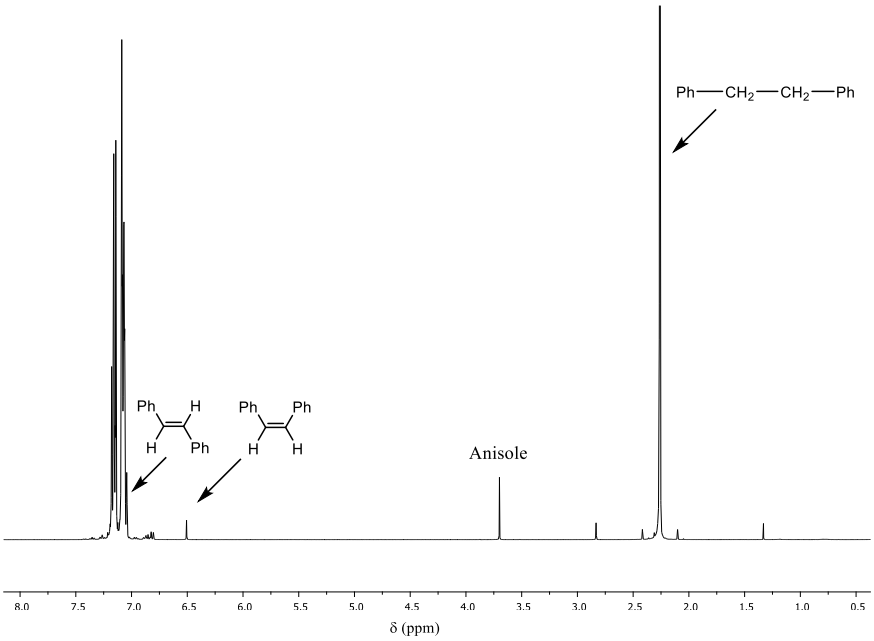

Figure S13 NMR spectra for hydrogenation reactions using diphenylacetylene as substrate:

S3. High Resolution Mass Spectroscopy (HRMS)

Mass spectra were obtained using a QTOF Premier (quadrupole-hexapole-TOF) with an orthogonal Z-spray-electrospray interface (Waters, Manchester, UK). The drying gas as well as nebulizing gas was nitrogen at a flow of 400 L/h and 80 L/h respectively. The temperature of the source block was set to 120 ^{o}C and the desolvation temperature to 150 ^{o}C. A capillary voltage of 3.5 KV was used in the positive scan mode and the cone voltage was set to 10 V to control the extent of fragmentation. Mass calibration was performed using a solution of sodium iodide in isopropanol:water (50:50) from m/z 150 to 1000 Da. Sample solutions (ca. 1 x 10^{-5} M) were infused via syringe pump directly connected to the interface at a flow of 10 μl/min. A 1 μg/mL solution of Luekine-enkephaline was used as lock mass for accurate m/z determinations.

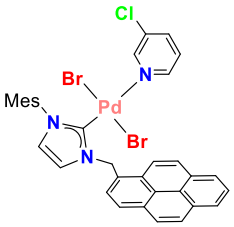

MW = 780.3 g/mol

Fragment: 700.0141 $[M - Br]^+$
732.0458 $[M-Br+MeOH]^+$

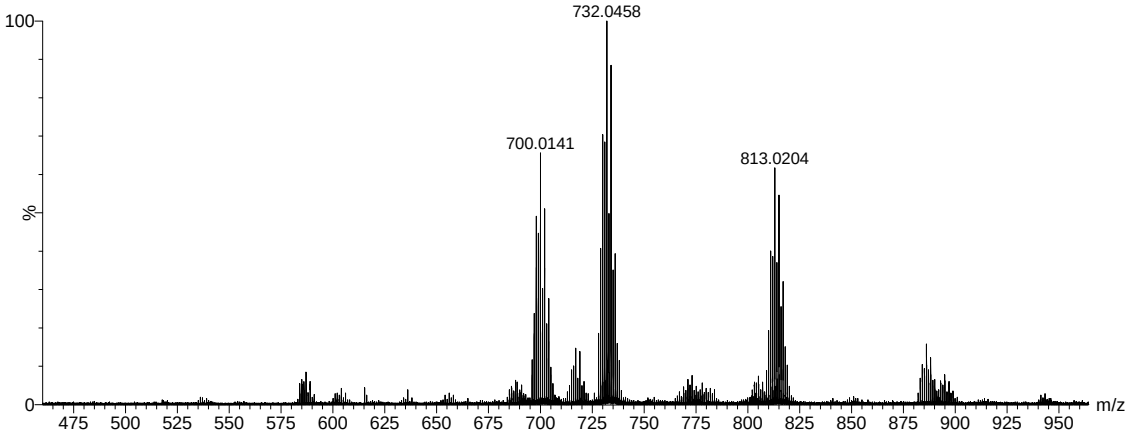

Simulated mass

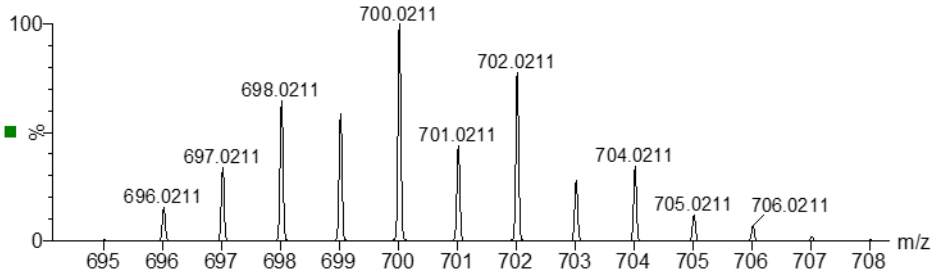

Experimental mass

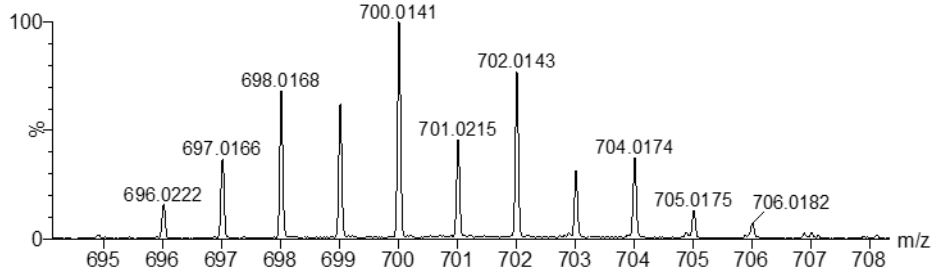

Peak (m/z)	Experimental mass	Theoretical mass	Relative error (ppm)
700.01	700.0141	700.0211	1

Figure S14 HRMS of complex **2**

S4. Single crystal X-Ray Diffraction Studies

S4.1 Crystal data of complex 2

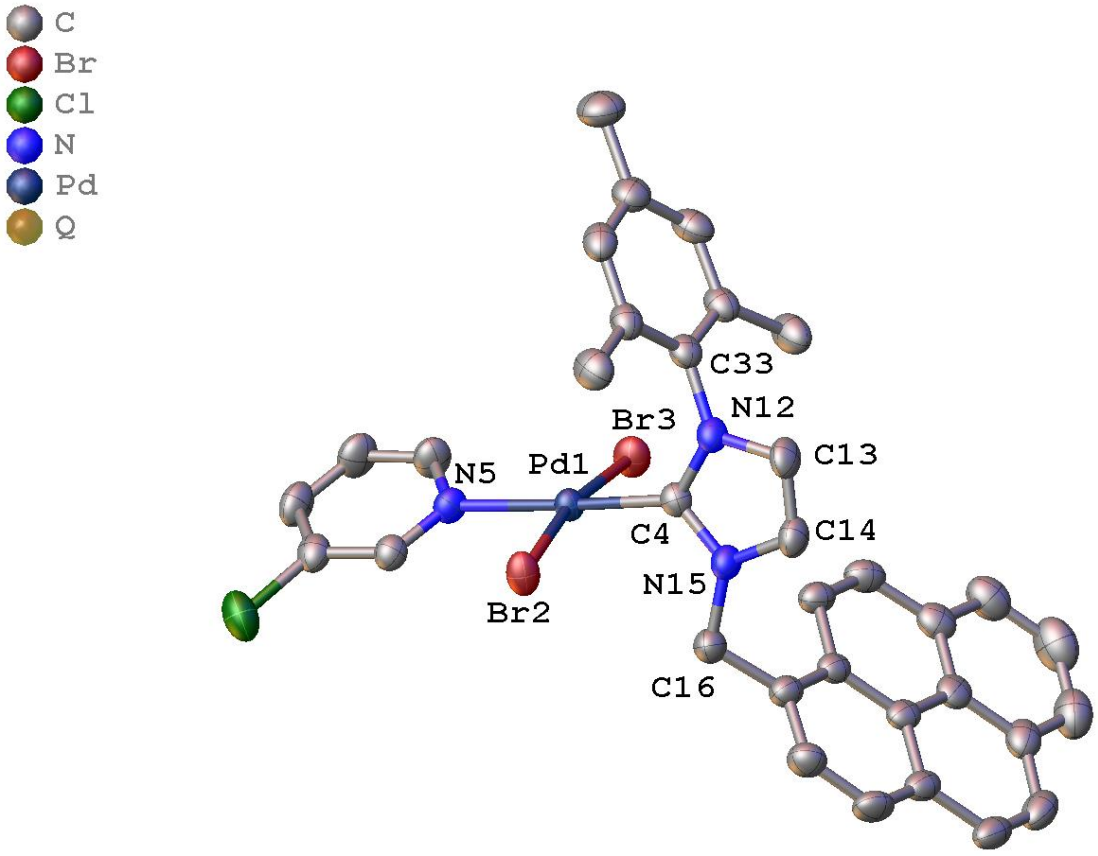

Figure S15 Molecular diagram of complex **2**

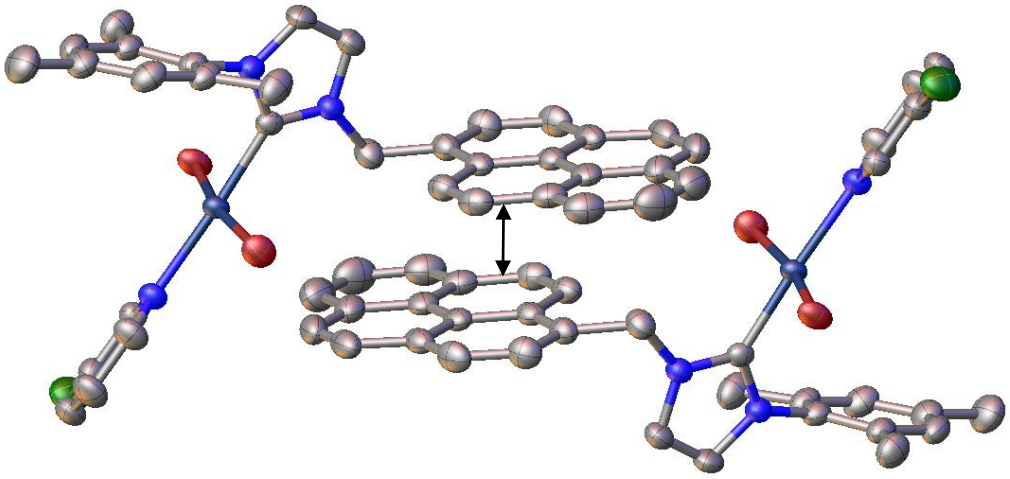

Figure S16 Packing diagram of complex **2** showing an interplanar distance between the pyrenes of 3.5 Å.

Table S1 Crystal data and structure refinement for complex **2**

CCDC Number	1838639
Identification code	ov_str1874
Empirical formula	$C_{34}H_{28}Br_2ClN_3Pd$
Formula weight	780.30
Temperature/K	293(2)
Crystal system	triclinic
Space group	P-1
a/Å	9.14864(16)
b/Å	11.5032(2)
c/Å	15.6073(3)
α/°	72.6495(16)
β/°	81.6726(15)
γ/°	72.6336(16)
Volume/Å^3	1493.47(5)
Z	2
ρ_{calc}g/cm^3	1.7351
μ/mm^{-1}	3.415
F(000)	769.5
Crystal size/mm^3	0.12 × 0.10 × 0.07
Radiation	Mo Kα (λ = 0.71073)
2Θ range for data collection/°	5.78 to 52.74
Index ranges	-11 ≤ h ≤ 11, -14 ≤ k ≤ 14, -19 ≤ l ≤ 19
Reflections collected	60406
Independent reflections	6105 [R_{int} = 0.0484, R_{sigma} = 0.0212]
Data/restraints/parameters	6105/0/372
Goodness-of-fit on F^2	1.064
Final R indexes [I>=2σ (I)]	R_1 = 0.0269, wR_2 = 0.0655
Final R indexes [all data]	R_1 = 0.0336, wR_2 = 0.0708
Largest diff. peak/hole / e Å^{-3}	0.59/-0.49

S5. Characterization of 2-rGO

S5.1 Thermogravimetric analysis of complex 2, rGO and the hybrid material 2-rGO

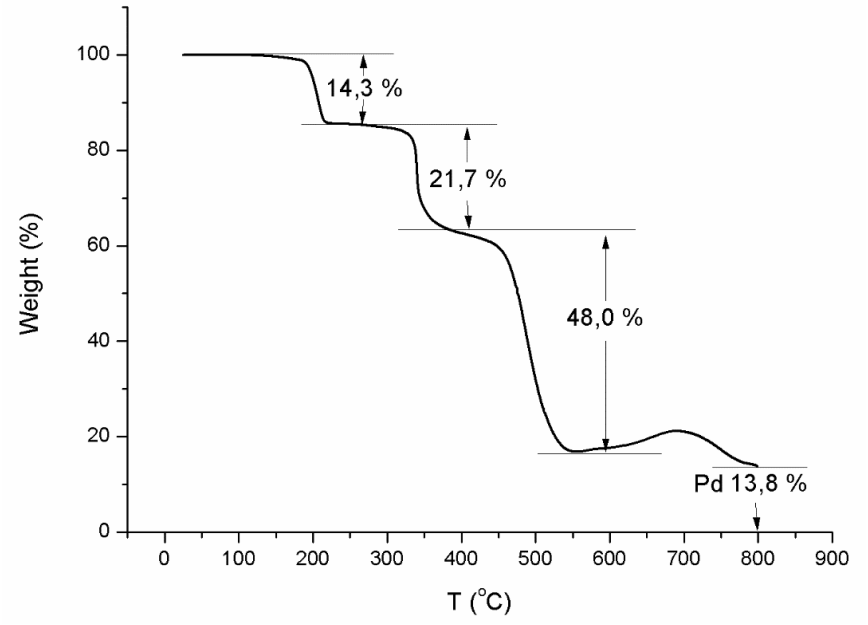

Figure S17 Termogravimetric analysis (TG) of **2**. TG analysis shows sequential mass losses that are assigned to the different palladium ligands. At 229 °C, the weight lost is 14,3 % that corresponds to 3-chloropyridine (14.5 % theo). At 380 °C, there is a weight lost of 21.7 % assigned to the two Br ligands (20.4 % theo). At 565 °C, the weight lost of the NHC ligand (48 % exp; 51,4 % theor.). At this temperature, there is 16 % of inorganic mass that corresponds to the remaining Pd. This reacts with oxygen to form PdO/PdO_2 (21 % exp, 18% teor.). At 800 °C, the % of inorganic mass is 13,8 % that is in agreement with the theoretical value of 13,4 % of metallic palladium.

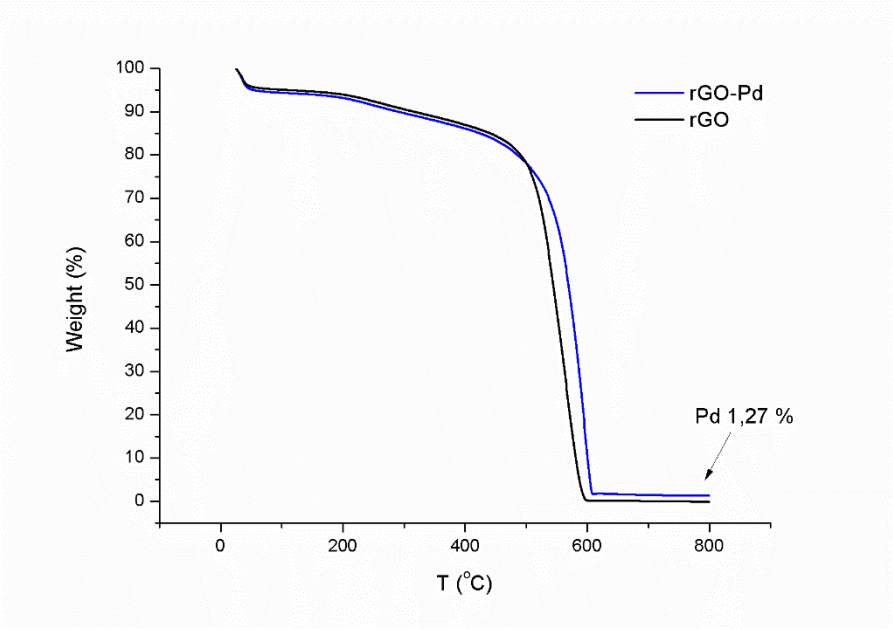

Figure S18 Comparative thermogravimetric analysis (TG) of **rGO** (black) and **2-rGO** (Blue).

S5.2 UV/Vis spectroscopy.

The UV/Vis spectra were recorded between 250 and 600 nm by a Cary 300 Bio UV−Vis Varian spectrophotometer. The samples were suspended in CH_2Cl_2 and sonicated for 5 minutes before the measurements.

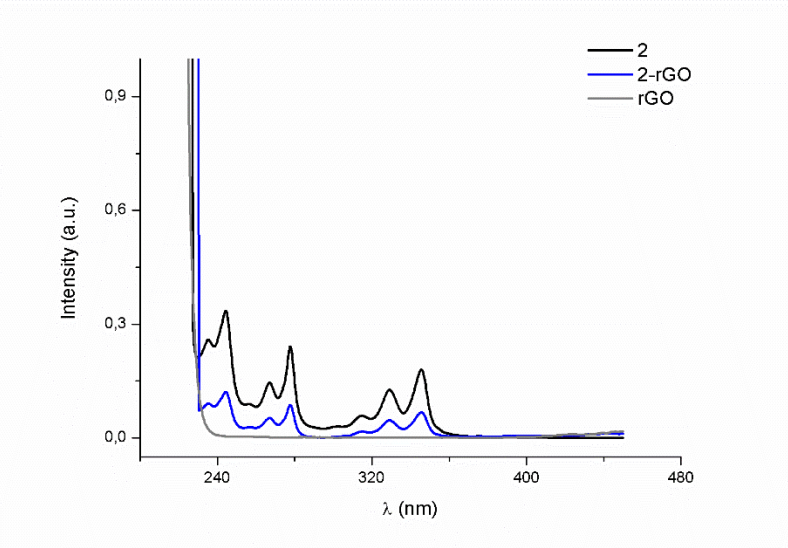

Figure S19 UV/Vis of palladium complex **2** (black), hybrid material **2-rGO** (blue) and **rGO** (grey)

S6. Raman spectroscopy

The Raman spectra of **2-rGO** exhibits a typical graphene-like pattern with characteristic D and G bands, attributed to sp^3 bonds (or the disorder in sp^2-hybridized bonds) and sp^2 bonds, respectively. The relative intensity of both bands (I_D/I_G) is often applied as an indicator for the extent of defects occurring on graphene materials. The D/G intensity ratios of the hybrid material **2-rGO** is slightly larger than rGO (1.40). This suggests the appearance of more defects over the rGO surface, and reflects a degree of functionalization.

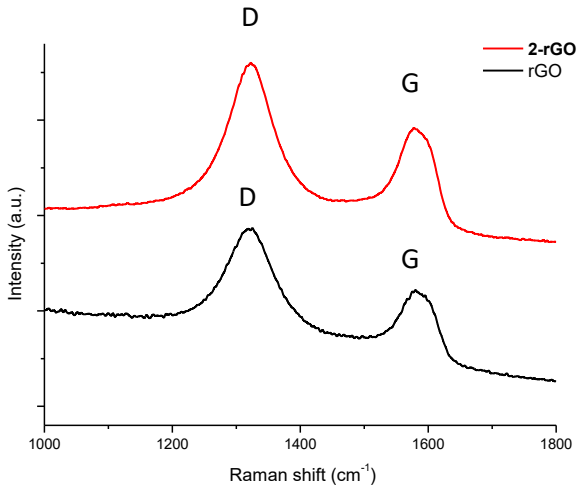

Figure S20 Raman spectra recorded using a 633 nm laser excitation

D/G intensity ratios of rGO and the hybrid material.

Material	I_D/I_G
rGO	1.40
2-rGO	1.42

S7. X-ray photoelectron spectroscopy (XPS)

X-ray photoelectron spectroscopy (XPS) spectra were acquired on a Kratos AXIS ultra DLD spectrometer with a monochromatic Al Kα X-ray source (1486.6 eV) using a pass energy of 20 eV. The photoelectron take off angle was 90^{o} with respect to the sample plane. To provide a precise energy calibration, the XPS binding energies were referenced to the C1s peak at 284.6 eV.

S7.1 Comparative XPS analysis of complex 2 and the hybrid material 2-rGO

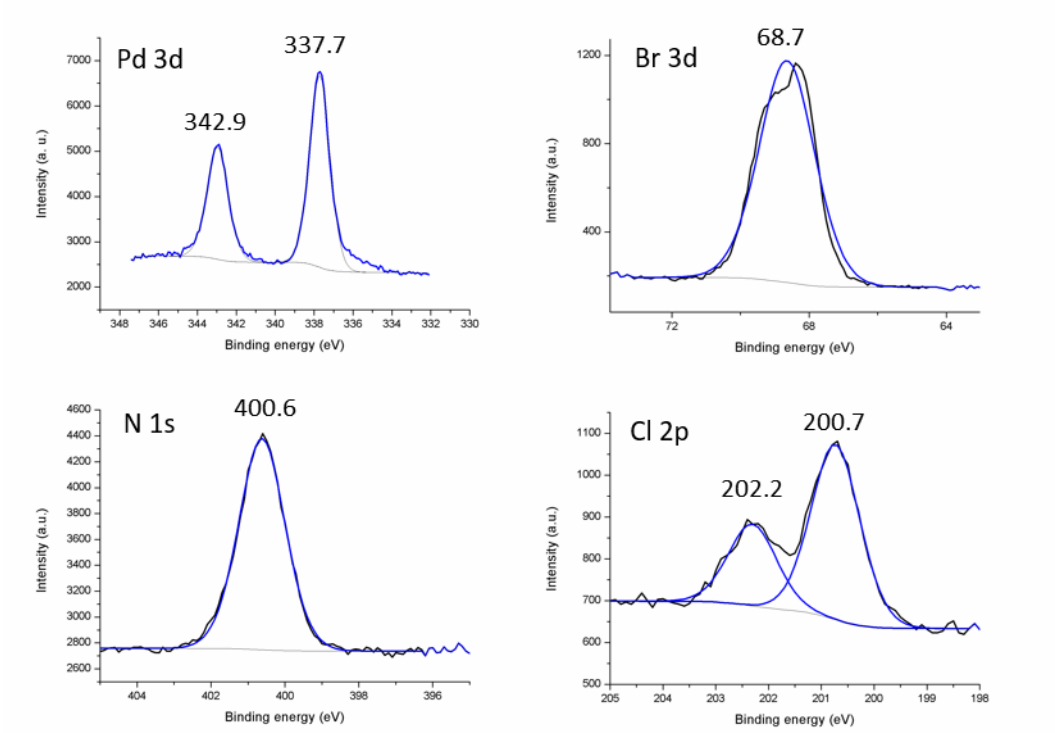

(a)

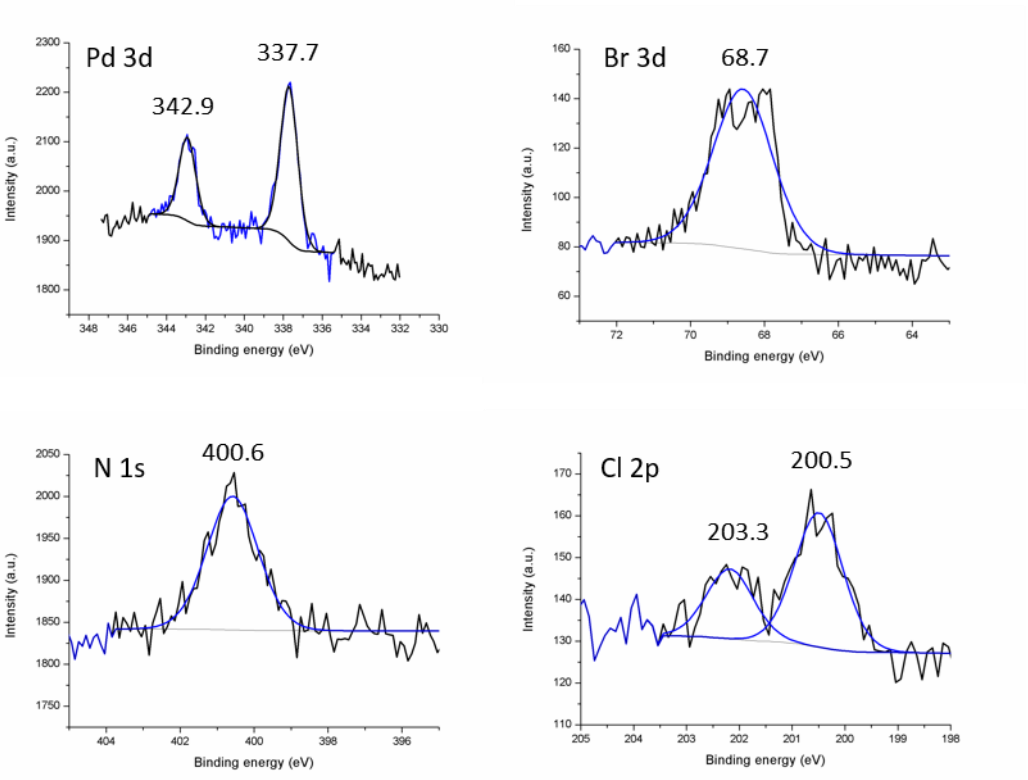

(b)

Figure S21 Comparative XPS analysis of molecular complex **2** (a) and hybrid material **2-rGO** (b) for the core-level peaks of Pd 3d, Br 3d, N 1s and Cl 2p. Binding energies in eV.

S8. High Resolution Transmission Electron Microscopy (HRTEM) images

High-resolution images of transmission electron microscopy HRTEM and high-angle annular dark-field HAADF-STEM images of the samples were obtained using a Jem-2100 LaB6 (JEOL) transmission electron microscope coupled with an INCA Energy TEM 200 (Oxford) energy dispersive X-Ray spectrometer (EDX) operating at 200 kV. Samples were prepared by drying a droplet of a MeOH dispersion on a carbon-coated copper grid.

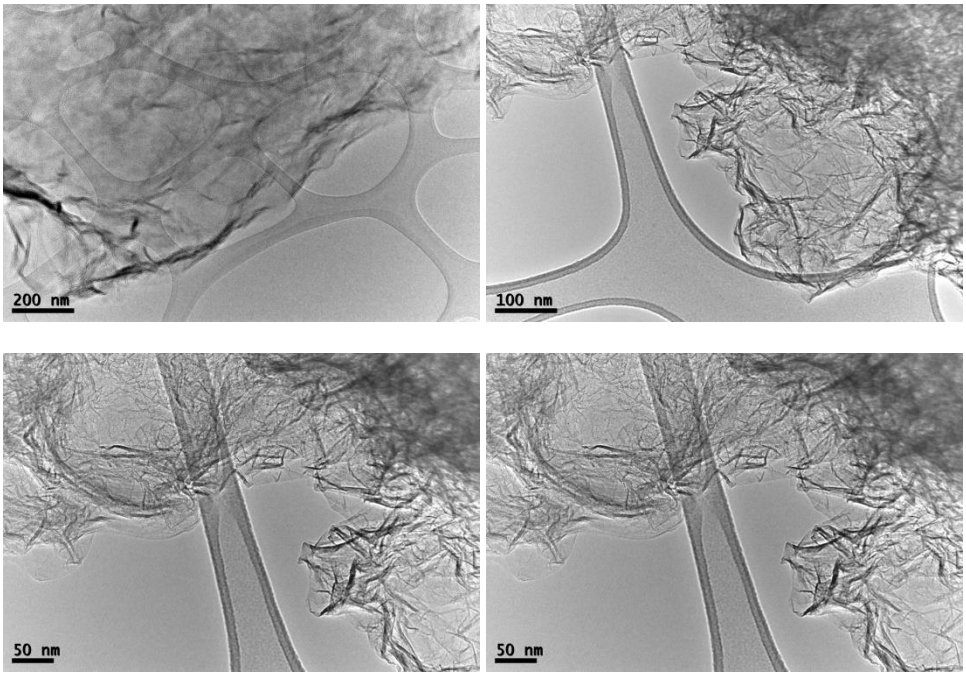

Figure S22 HRTEM images of **2-rGO** at different magnifications

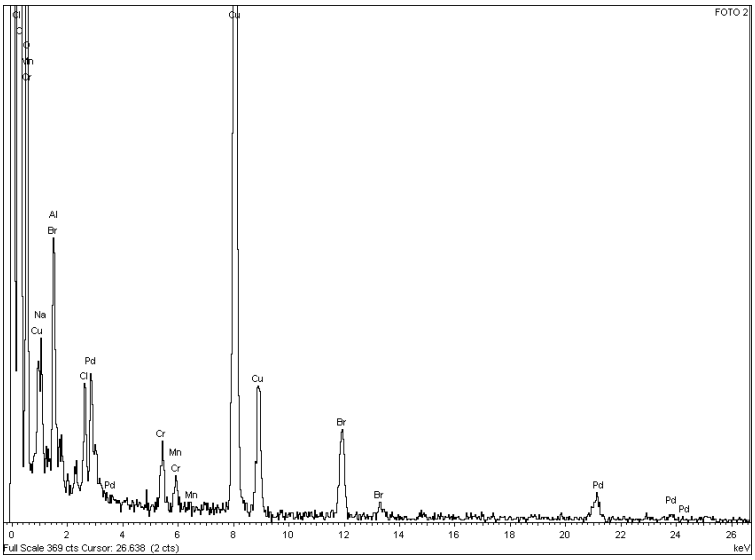

Figure S23 EDS analysis of **2-rGO** showing the presence of Pd and Br. The TEM grid causes the presence of copper, and the components of the microscope lenses cause the presence of chromium. Manganese is a contamination coming from the synthetic procedure. In the preparation of rGO, Graphite is oxidized by the Hummers method using $KMnO_4$. We have evidence that Mn is not a catalytic active species because blank experiments using only rGO are inactive in the hydrogenation reactions.

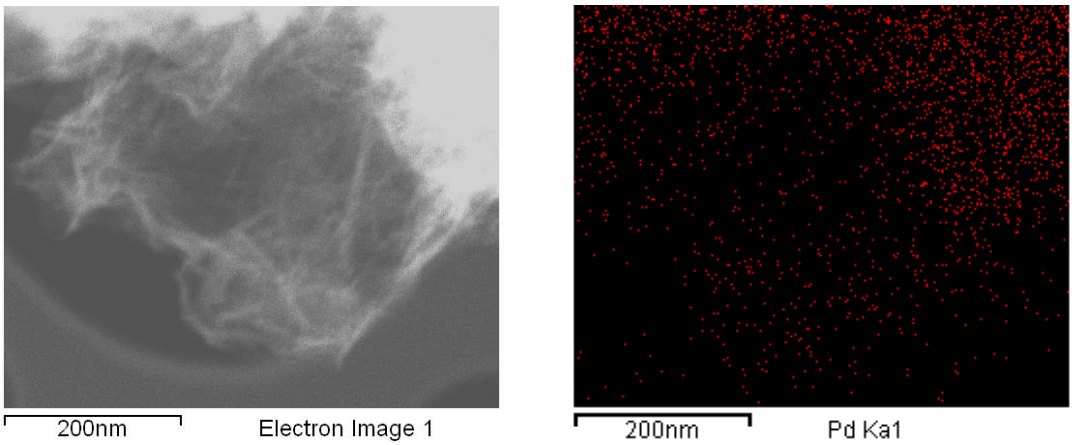

Figure S24 STEM image of **2-rGO** (left) and EDS elemental mapping image showing the homogeneous distribution of palladium (right).

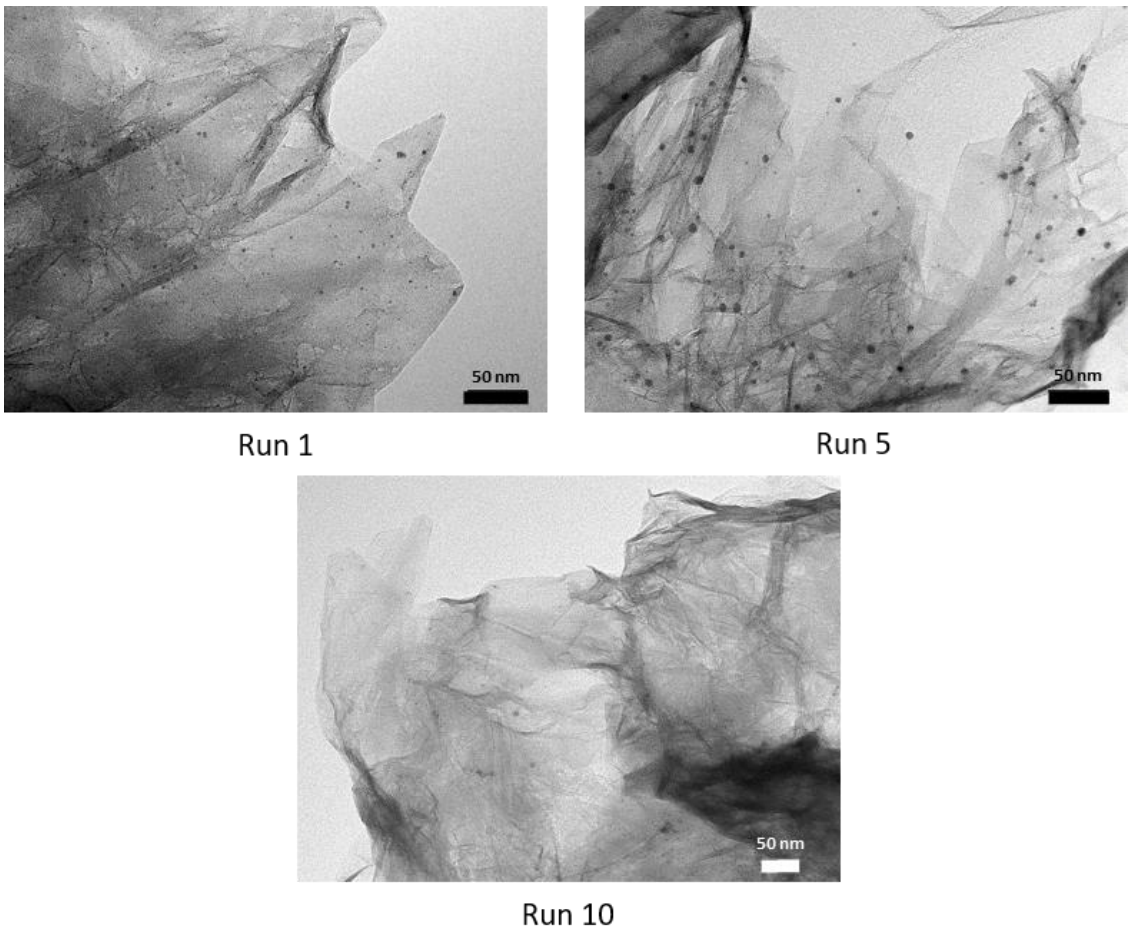

Figure S25 HRTEM images of **2-rGO** after runs 1, 5 and 10 during the recycling experiment showing the presence of palladium nanoparticles.

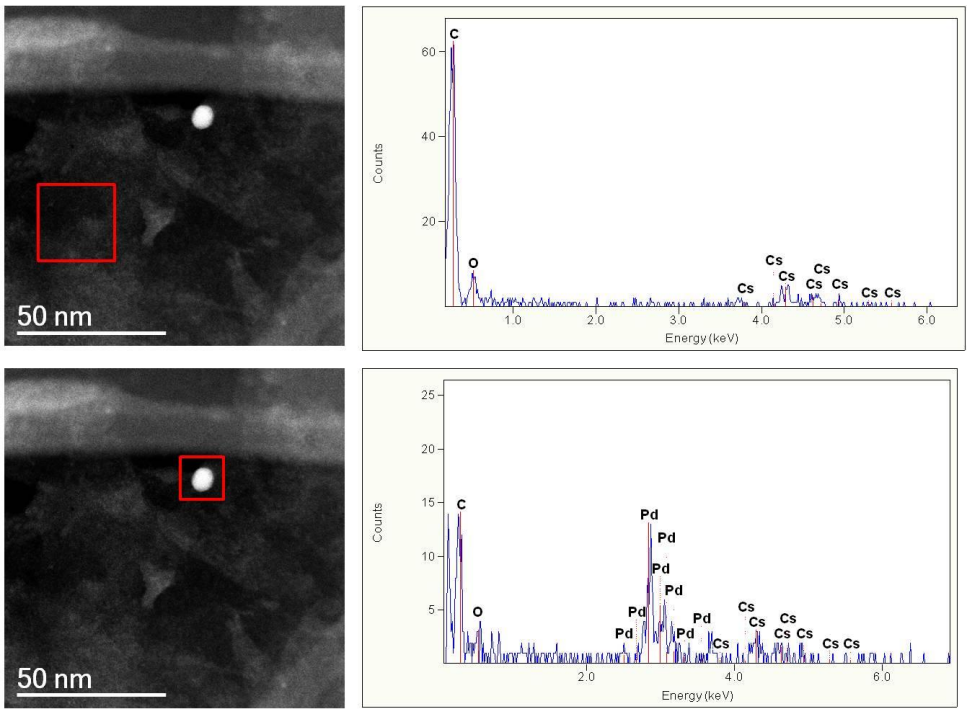

Figure S26 Spherical aberration (C_s) corrected STEM image (left) and EDX spectrum of selected regions (right) shows the presence of cesium in the form of individual atoms and palladium nanoparticles in the **2-rGO-NPs**.

S9. Poisoning experiments

Poisoning experiments using P4VP (poly(4-vinylpyridine)) as an scavenger of Pd(II) molecular species and the Hg drop test as an scavenger of Pd nanoparticles. Scavengers added after 30 min reaction to assure the formation of the catalytic active species.

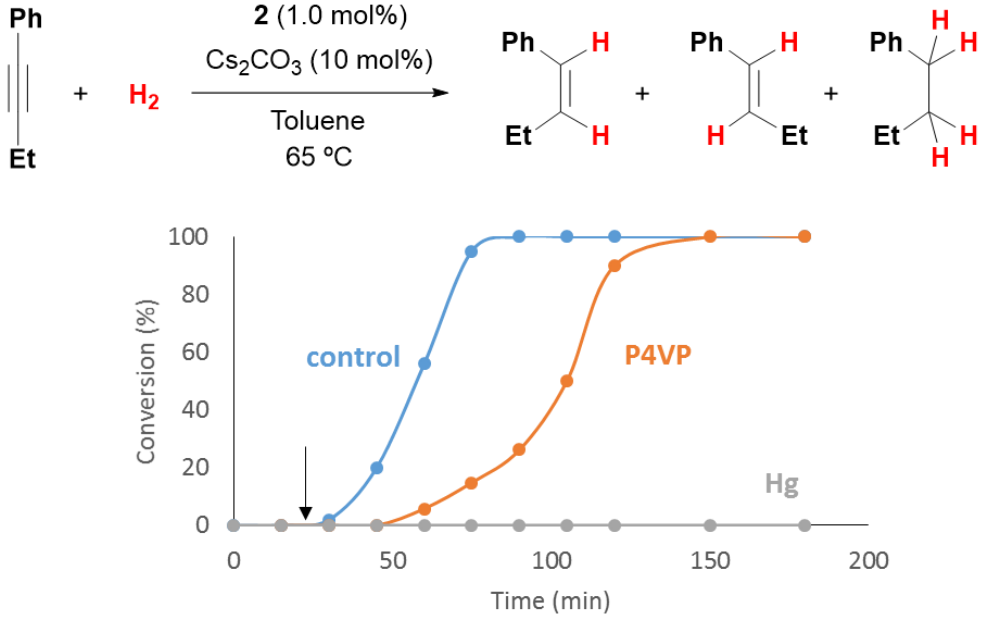

Figure S27 Poisoning experiments using poly(4-vinylpyridine) (orange line) or Hg (grey line).

The Maitlis hot filtration test. This test involves the filtration of a part of the catalytic reaction maintaining the reaction conditions and monitoring the reaction time-profile in the remaining solution and the filtrate. No catalytic activity in the filtrate suggests heterogeneous active catalytic species. In the hydrogenation of 1-phenyl-1-butyne with precatalyst **2**, after 1 h reaction (GC conversion 40 %) half of the reaction mixture was filtered off through celite at 65 °C. The filtrate was maintained for 5 h under identical conditions, but GC analysis indicated that no further hydrogenation occurred (GC conversion 40%). On the contrary, the remaining mixture achieved full conversion in 2 h reaction.

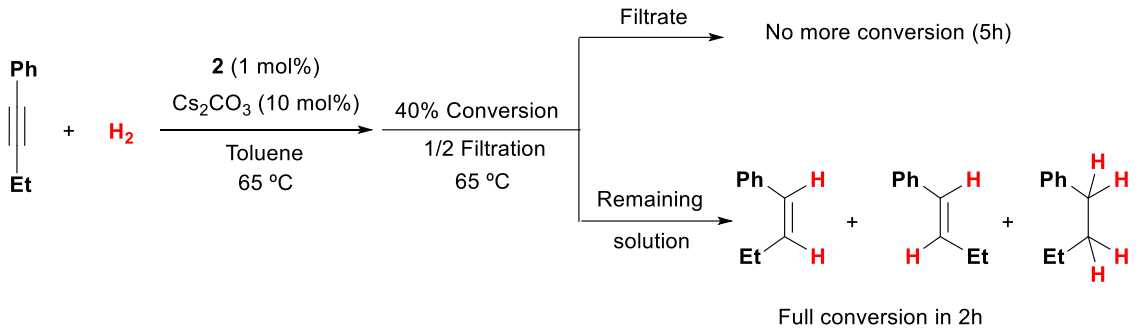

S10. Hydrogenation competitive experiments

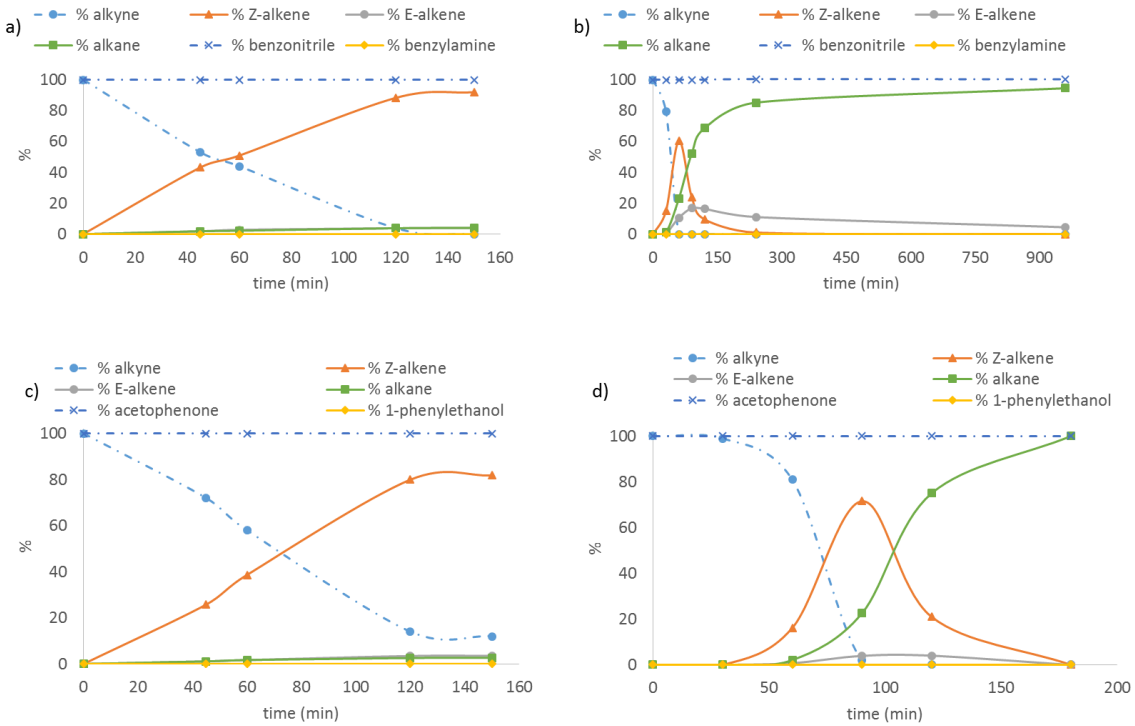

Figure S28 Competitive experiment in the hydrogenation of 1-phenyl-1-butyne in the presence equimolar amounts of benzonitrile using catalyst a) **2** (1 mol %) and b) **2-rGO** (0.5 mol%) or acetophenone using catalyst c) **2** (1 mol %) and d) **2-rGO** (0.5 mol%).

S11. Hydrogenation reaction monitoring for substrates of Table 1.

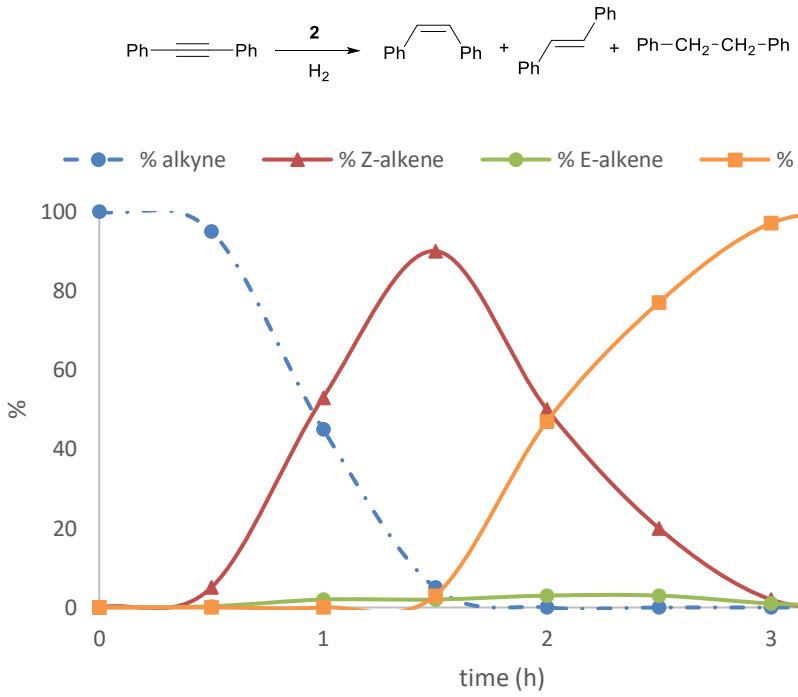

Figure S29 Hydrogenation of diphenylacetylene with **2** (Table 1, entry 1).

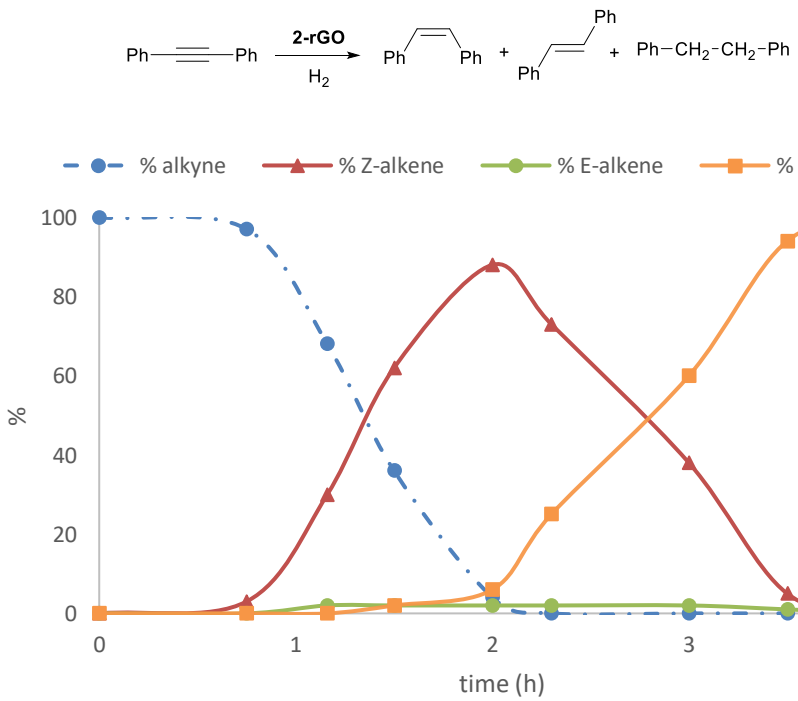

Figure S30 Hydrogenation of diphenylacetylene with **2-rGO** (Table 1, entry 2).

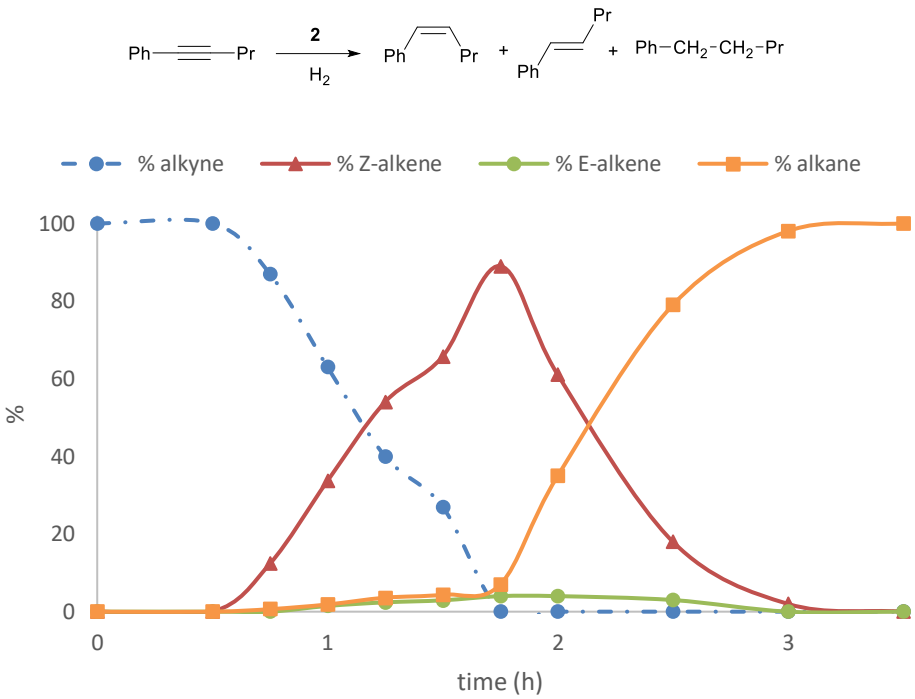

Figure S31 Hydrogenation of 1-phenyl-1-pentyne with **2** (Table 1, entry 3).

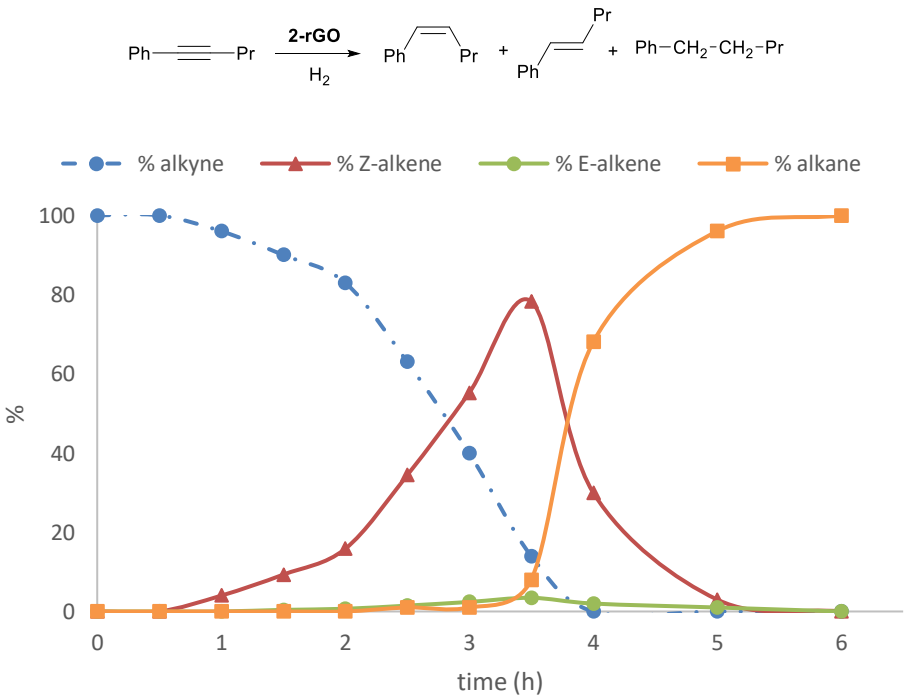

Figure S32 Hydrogenation of 1-phenyl-1-pentyne with **2-rGO** (Table 1, entry 4).

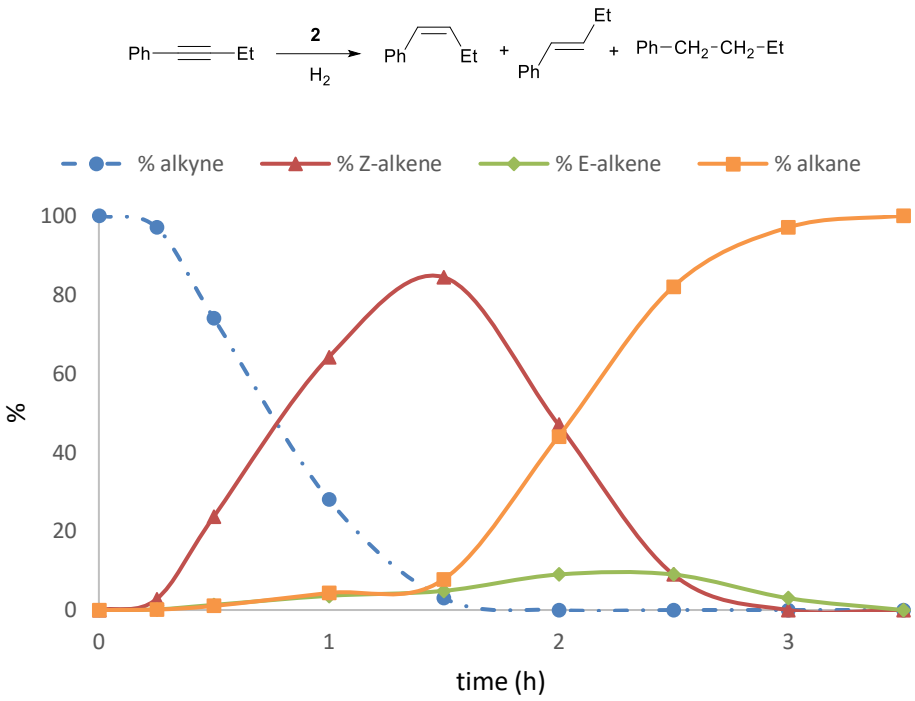

Figure S33 Hydrogenation of 1-phenyl-1-butyne with **2** (Table 1, entry 5).

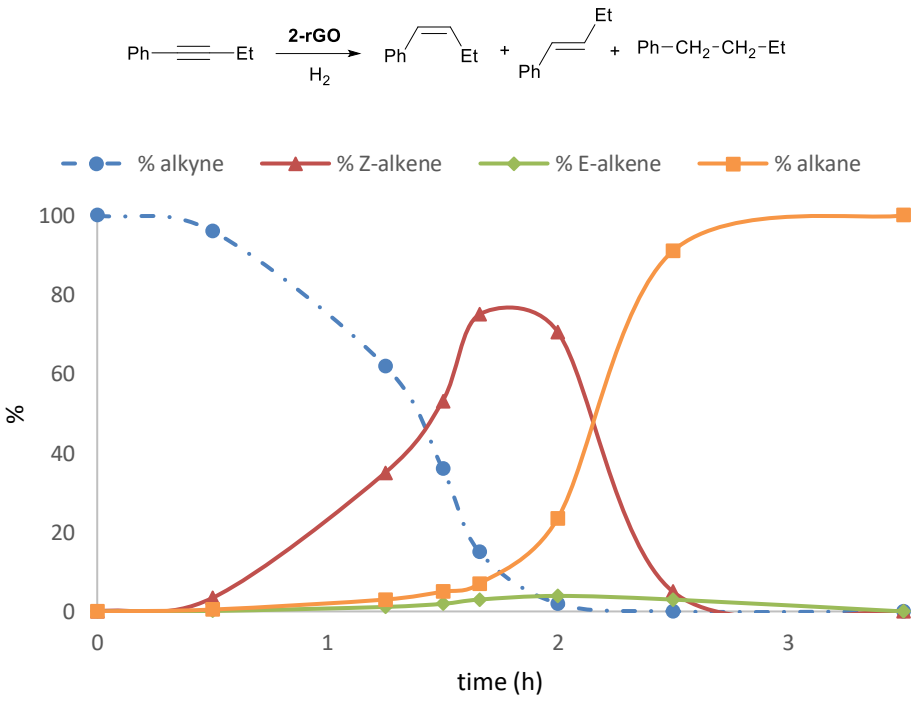

Figure S34 Hydrogenation of 1-phenyl-1-butyne with **2-rGO** (Table 1, entry 6).

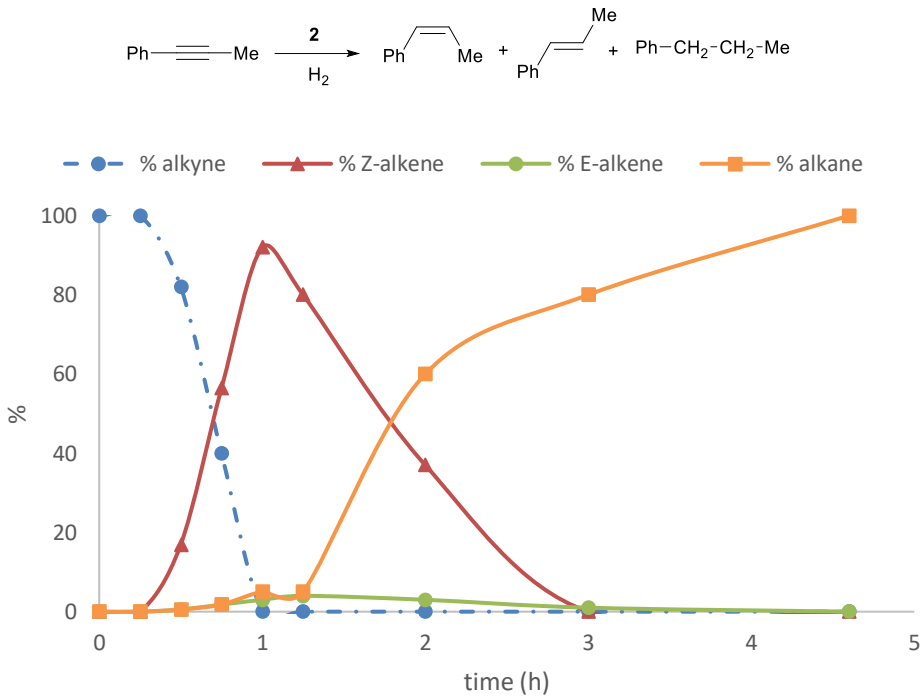

Figure S35 Hydrogenation of 1-phenyl-1-propyne with **2** (Table 1, entry 7).

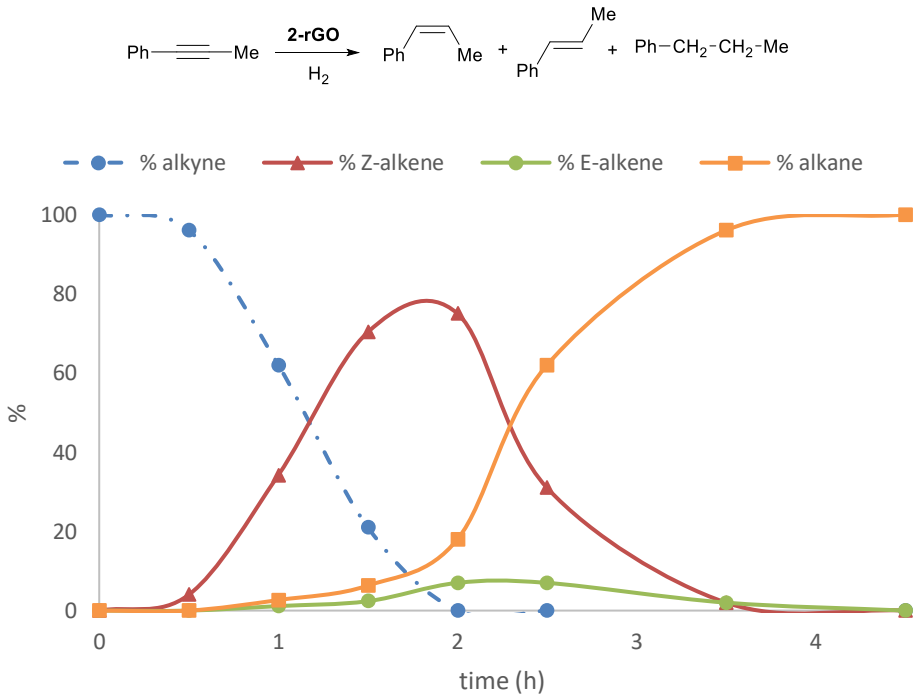

Figure S36 Hydrogenation of 1-phenyl-1-propyne with **2-rGO** (Table 1, entry 8).

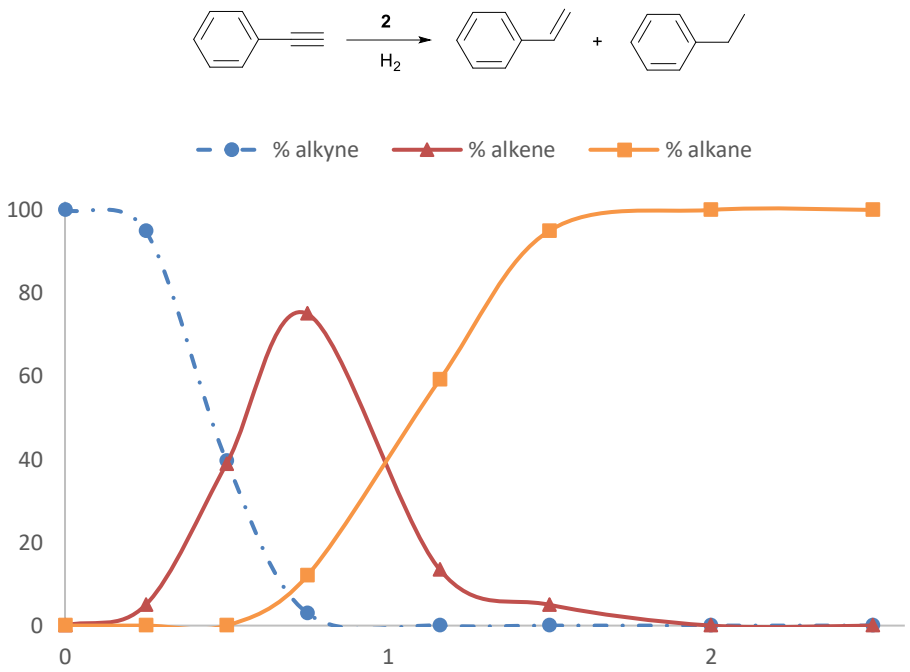

Figure S37 Hydrogenation of phenylacetylene with **2** (Table 1, entry 9).

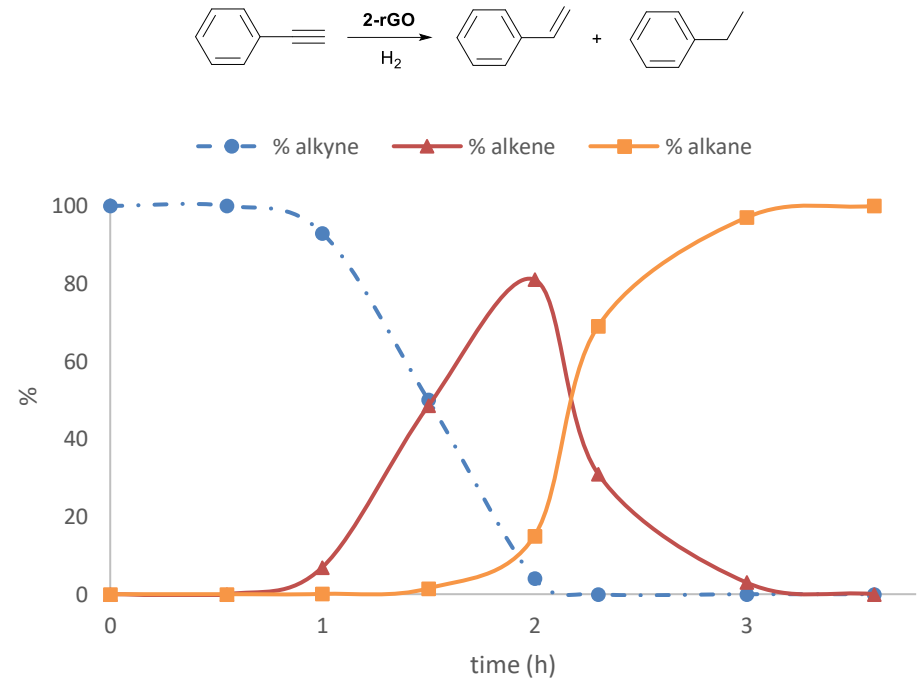

Figure S38 Hydrogenation of phenylacetylene with **2-rGO** (Table 1, entry 10).

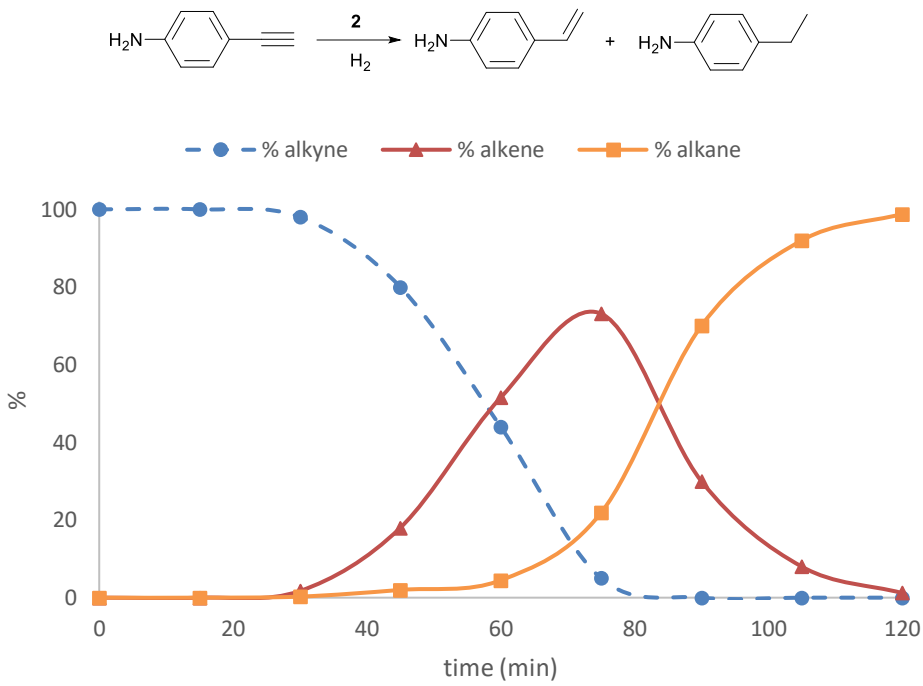

Figure S39 Hydrogenation of 4-ethynylaniline with **2** (Table 1, entry 11).

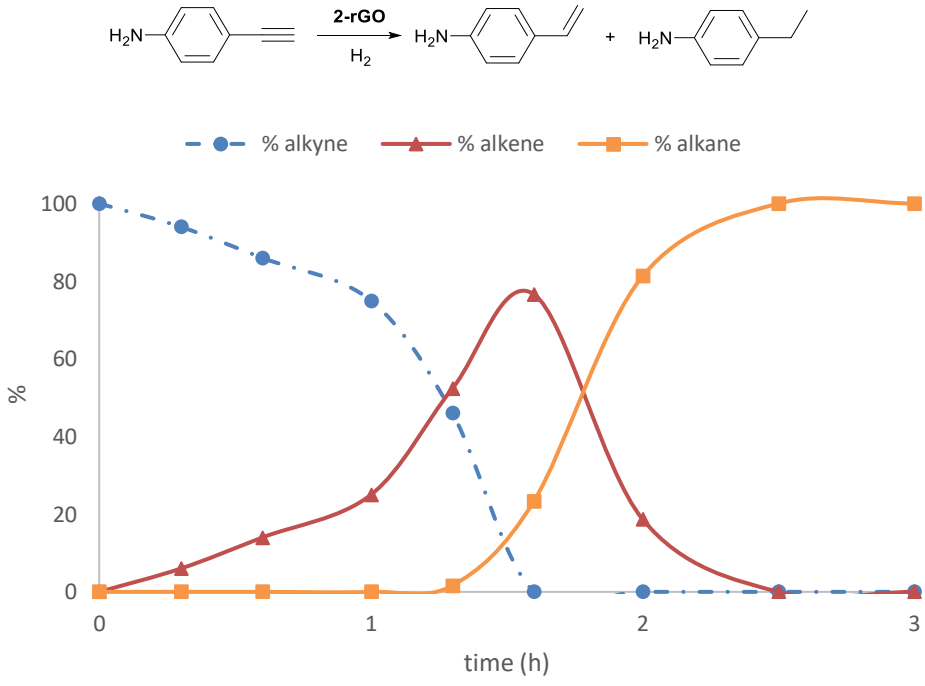

Figure S40 Hydrogenation of 4-ethynylaniline with **2-rGO** (Table 1, entry 12).